Electronic Supplementary Information

Ultrafast ion-exchange synthesis of 3D lithiophilic scaffolds for high-capacity anode-less all-solid-state batteries

Jihoon Oh,[a,b] Taegeun Lee,[a,b] Noh Joon Lee,[a,b] Yeeun Sohn,[a,b] Sanghun Park,[a,b] Ji Young Kim,[c] Ki Yoon Bae,[c] and Jang Wook Choi*[a,b,d]

[a] *School of Chemical and Biological Engineering and Institute of Chemical Process, Seoul National University, Seoul, Republic of Korea. E-mail: jangwookchoi@snu.ac.kr*
[b] *Hyundai Motor Group-Seoul National University (HMG-SNU) Joint Battery Research Center (JBRC), Seoul National University, Seoul, Republic of Korea*
[c] *Advanced Battery Development Team, Hyundai Motor Company, Hwaseong-si, Republic of Korea*
[d] *Seoul National University Energy Initiative (SNUEI), Seoul National University, Seoul, Republic of Korea.*
† Electronic Supplementary Information (ESI) available: See DOI: 10.1039/x0xx00000x

Experimental Section

Electrode Preparation: The Ni layer was fabricated using a slurry casting technique. Commercially acquired Ni nanopowder (particle size D50 = 20 nm) was mixed with Spandex binder in a weight ratio of 96:4, utilizing *N*-methyl-2-pyrrolidone (NMP) as the solvent. The resulting slurry was uniformly cast onto a stainless steel (SUS) substrate employing the doctor blade method. Subsequently, the Ni layer was dried in a vacuum chamber at 60 °C for 12 hours to ensure complete solvent removal. The p-Ag-Ni layer was synthesized via a facile ion-exchange method. A Ni layer with a diameter of 10 mm was immersed in 1 mL of aqueous $AgNO_3$ solution for 30 seconds while being agitated on an orbital shaker at 300 rpm to ensure uniform ion exchange. Following the reaction, the disc was washed thrice with 10 mL of deionized (DI) water. Subsequent drying at 100 °C for 6 hours resulted in a p-Ag-Ni layer with a consistent thickness of approximately 20 μm (3.0 mg cm^{-2}). For the fabrication of powder-cast control samples, Ag nanoparticles (Alfa Aesar, D50 = 30 nm), Ag nanowires (Novarials, 100 nm × 10 μm), and Mg nanoparticles (Avention, D50 = 800 nm) were used. Each powder was combined with a PVDF (Kynar) binder in a 95:5 weight ratio using NMP as the solvent to prepare a homogeneous slurry, which was subsequently deposited onto SUS foil by doctor-blade coating and dried at 80 °C for 12 h. The thickness of all cast control layers was fixed at 20 μm, consistent with that of the p-Ag-Ni scaffold.

Cell Fabrication: Asymmetric anode-less|SE|Li half-cells were fabricated through a multi-step compression process. Initially, the LPSCl powder was compressed into a pellet with a diameter of 10 mm by applying 150 MPa. The premade p-Ag-Ni anode-less layer was then positioned on the SE pellet, followed by further compression at 400 MPa. Li metal foil was subsequently attached to opposite side of the pellet. The cell was then mounted in a housing case, tightened to 6 N m using a torque wrench, and an external pressure of 15 MPa was maintained during cell testing. All-solid-state full-cells were constructed using a similar methodology. The anode-less layer and cathode composites (prepared by mixing dry $LiNbO_3$-coated NCM811, LPSCl, and vapor-grown carbon fibers (VGCF) in a 70:28:2 weight ratio) were positioned on opposing sides of the SE pellet. The entire assembly was subjected to compression at 400 MPa, with the NCM811 achieving an areal mass loading of 20 mg_{NCM} cm^{-2}. All assembly procedures were conducted within an argon-filled glove box to minimize exposure to moisture and oxygen.

Electrochemical Characterization: The electrochemical performance of anode-less|SE|Li all-solid-state half-cells was comprehensively evaluated using a battery cycler (WBCS3000L, WonATech). Experimental parameters were established with current densities of 1 mA cm^{-2} and areal capacities of 1 mA cm^{-2} or 3.5 mAh cm^{-2}, with a potential cutoff of 0.1 V during the Li stripping process. The NCM|SE|anode-less all-solid-state full-cells were charged in constant current constant voltage (CCCV) mode, and discharged in constant current (CC) mode across a potential window of 2.5–4.2 V using the same battery cycler. The formation step involved initial cycling at a charge and discharge rate of 0.1C for one complete cycle. During the CCCV charging mode, the voltage was maintained constant at 4.2 V upon reaching this value and sustained until the current density decreased to 0.05C. The rate performance was tested during charge-discharge cycling at varying C-rates ranging from 0.1 to 0.5C in CCCV mode for charging and CC mode for discharging. All electrochemical measurements were conducted at a consistent temperature of 25 °C. The interfacial resistance of the anode-less|SE |Li all-solid-state half-cells was characterized by conducting EIS measurements using a battery cycler (VSP, Bio-Logic), and by sweeping a frequency range from 1 MHz to 1 Hz.

Characterization of Materials: The crystal structure and chemical composition of the p-Ag-Ni electrode were comprehensively investigated using XRD (New D8 Advance, Bruker) and XPS (PHI 5000 VersaProbe, ULVAC-PHI), respectively. The surface morphology was examined by acquiring top-view SEM (SEM-7800F Prime, Jeol) images. Cross-sectional imaging of the electrode involved precise dicing utilizing a cross-section polisher (CP; ArBlade 5000, Hitachi). Complementary elemental distribution was mapped using EDS (Ultim Extreme, Oxford Instruments). Advanced 3D characterization was conducted using an integrated high-resolution XRM computed tomography system (Xradia 620 Versa, Carl Zeiss, USA), located at the National Center for Inter-university Research Facilities (NCIRF) at Seoul National University. The anode and interface were selectively analyzed through X-ray beam exposure under precisely controlled conditions: 80 kV, 125 μA, and 10 W, with an image resolution of 0.7 pixels per unit over an 8-hour scanning period.

Pouch-Cell Fabrication Methodology: SE sheets containing LPSCl were prepared using butadiene rubber (BR) as a binder in butyl butyrate solvent. The materials were blended with zirconium dioxide (ZrO_2) beads using a planetary centrifugal mixer (Thinky Corporation, AR-100). The resultant mixture was uniformly coated onto a release-type polyethylene terephthalate (PET) film employing the doctor blade technique. The coated film underwent preliminary drying on a hotplate at 60 °C for several minutes, followed by extended drying in a vacuum oven at 40 °C overnight. The cathode was prepared via an identical slurry casting method by incorporating $LiNbO_3$-coated NCM811, LPSCl, VGCF, and BR binder in a weight ratio of 76:20:1.5:2.5, with a cathode mass loading of 20 mg_{NCM} cm^{-2}. These preparation steps were executed within a dry room maintained at a low dew point below −50 °C to minimize moisture contamination. A 15 × 15 mm^2 pouch-cell was fabricated using a systematic process. Electrodes and SE sheets were precision-cut using a punching machine and stacked within a laminate bag. After vacuum sealing, the assembly was subjected to high-pressure consolidation at 450 MPa and 75 °C for 30 minutes using a warm isostatic press (WIP; ISA-W50-6000, Ilshin Autoclave).

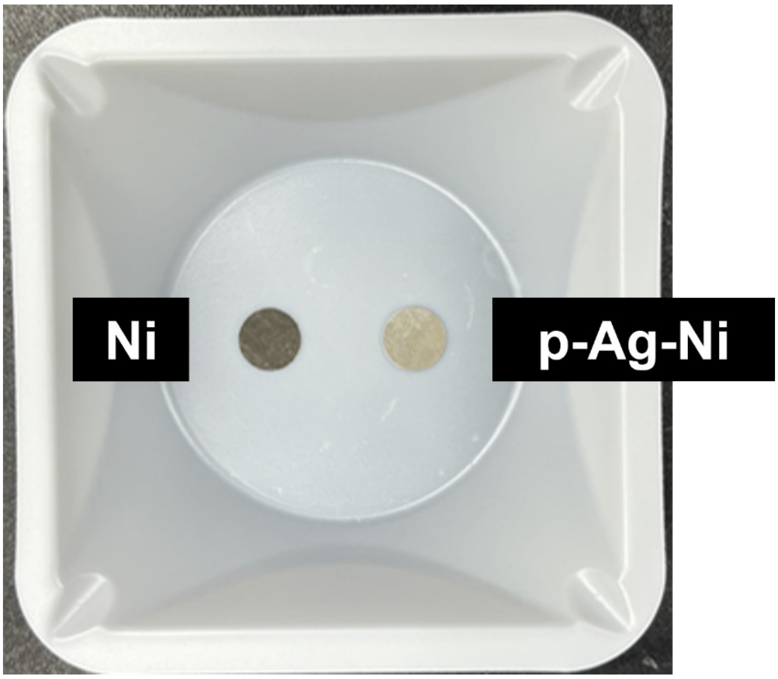

Fig. S1. Photograph of the bare Ni and p-Ag-Ni electrodes.

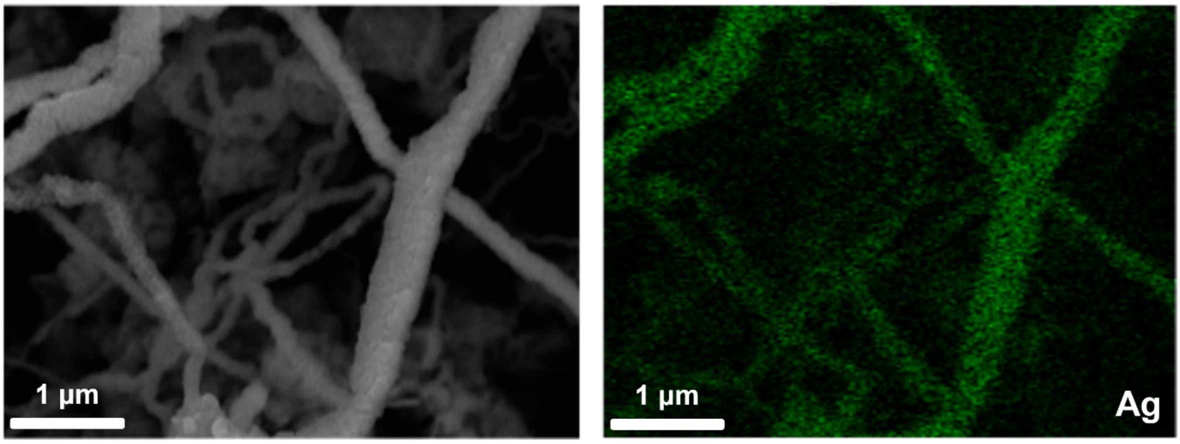

Fig. S2. SEM-EDS images of the p-Ag-Ni layer.

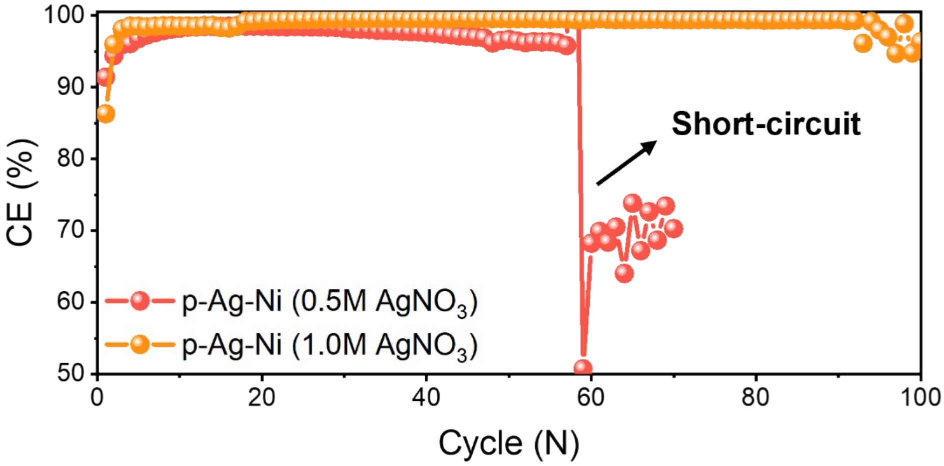

Fig. S3. Half-cell Li plating-stripping CEs of the p-Ag-Ni scaffolds fabricated with 0.5 M and 1 M $AgNO_3$ solutions.

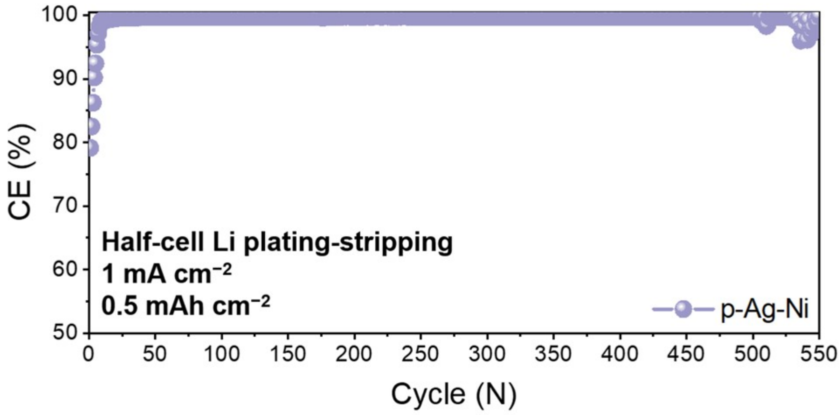

Fig. S4. Half-cell Li plating-stripping CEs at a current density of 1 mA cm^{-2} and a capacity of 0.5 mAh cm^{-2}.

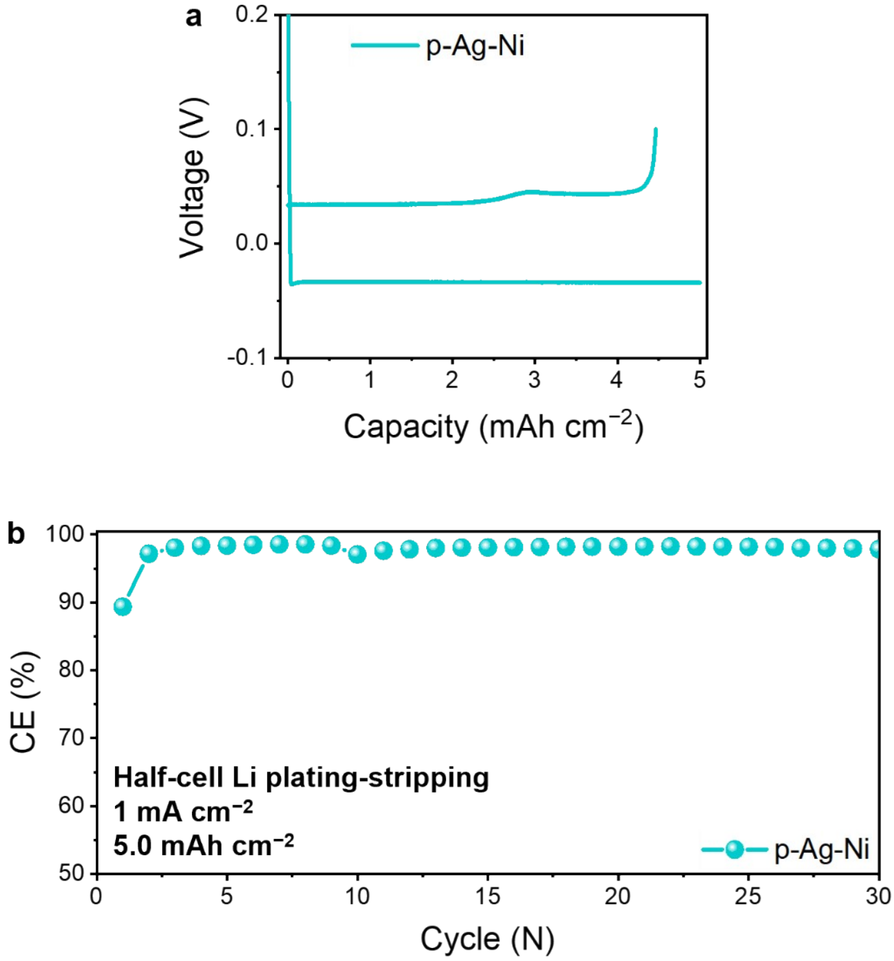

Fig. S5. Half-cell Li plating-stripping test of the p-Ag-Ni at a current density of 1 mA cm^{-2} and capacity of 5 mAh cm^{-2}: (a) Voltage profile of the first cycle and (b) CE.

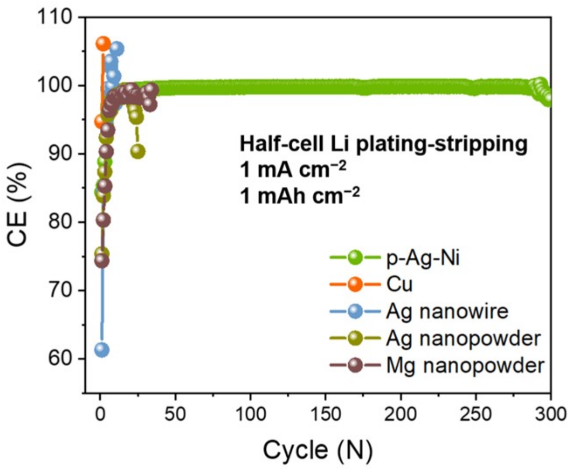

Fig. S6. Half-cell Li plating-stripping CEs of various anode-less configurations at a current density of 1 mA cm^{-2} and capacity of 1 mAh cm^{-2}.

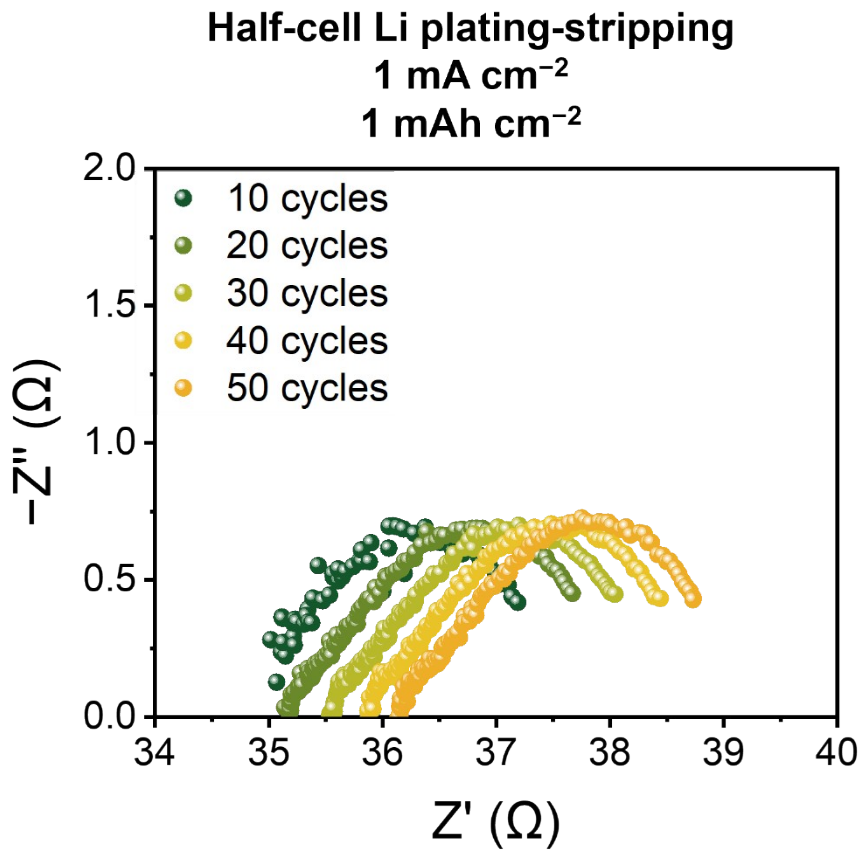

Fig. S7. Nyquist plots of the p-Ag-Ni-based half-cell after various Li plating-stripping cycles at a current density of 1 mA cm^{-2} and capacity of 1 mAh cm^{-2}.

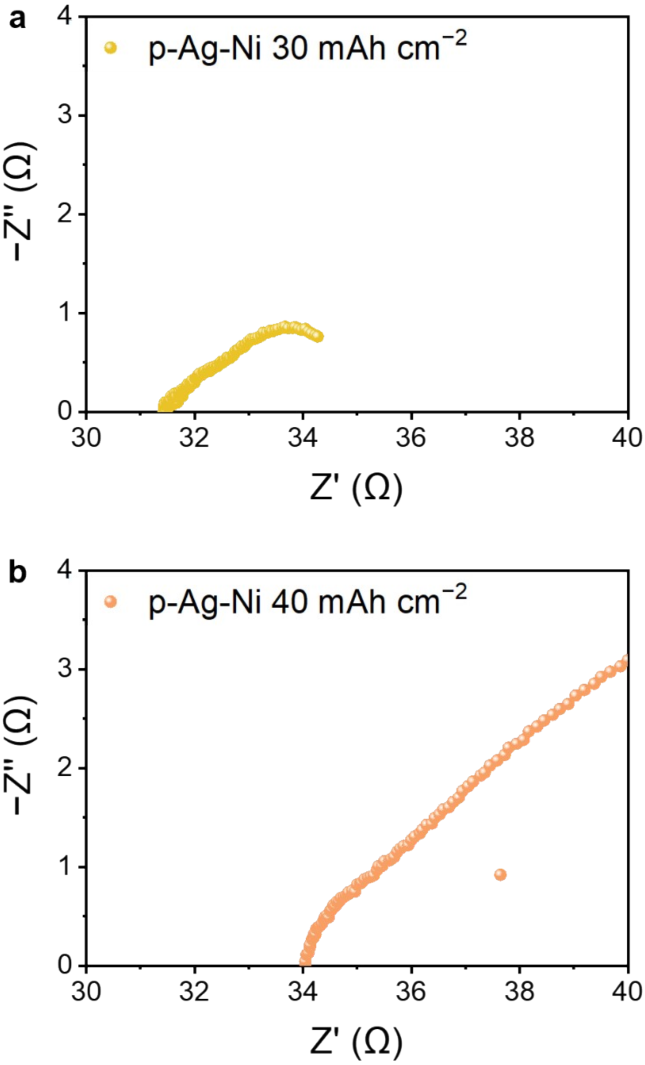

Fig. S8. Nyquist plots of in situ EIS measurements recorded during half-cell chronopotentiometry analyses, after Li plating of (a) 30 mAh cm^{-2} and (b) 40 mAh cm^{-2}.

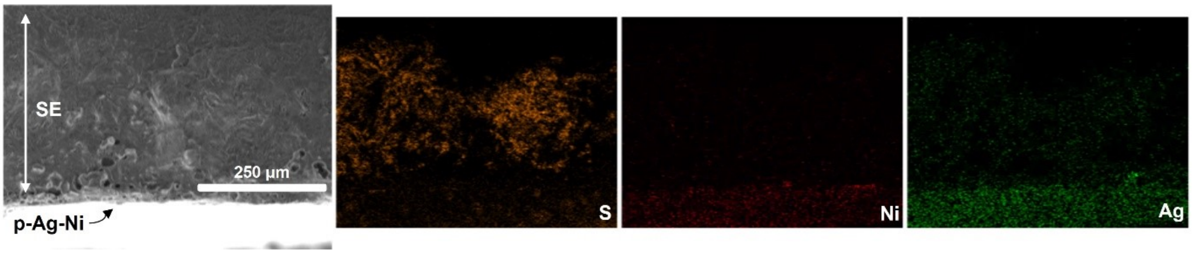

Fig. S9. Cross-sectional SEM-EDS images of the cell pellet after Li plating on p-Ag-Ni to a capacity of 35 mAh cm^{-2}.

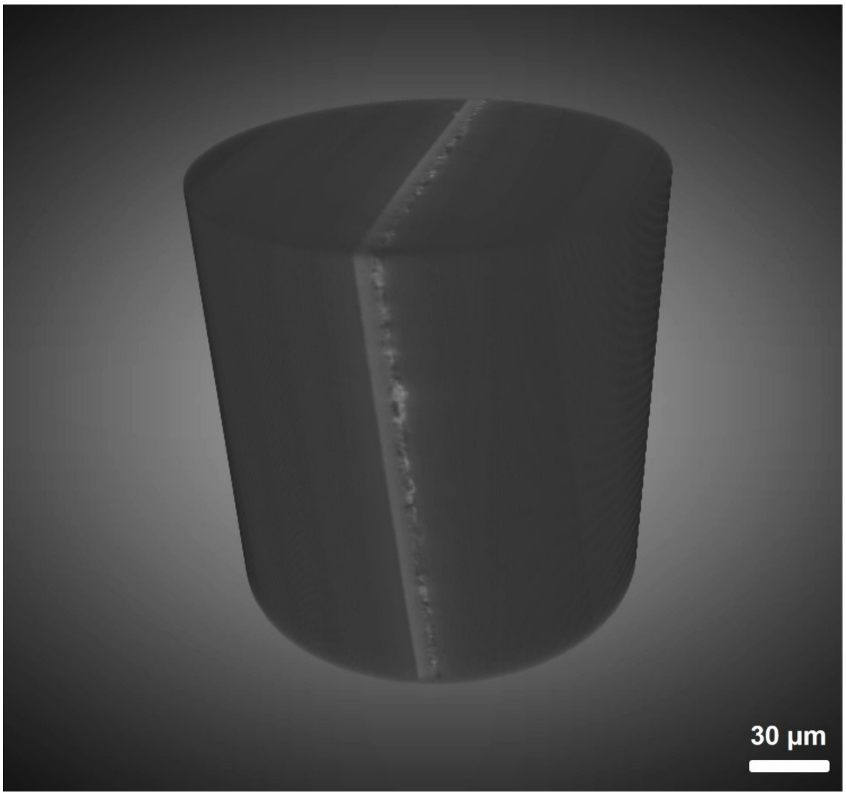

Fig. S10. XRM raw image of the pristine p-Ag-Ni layer.

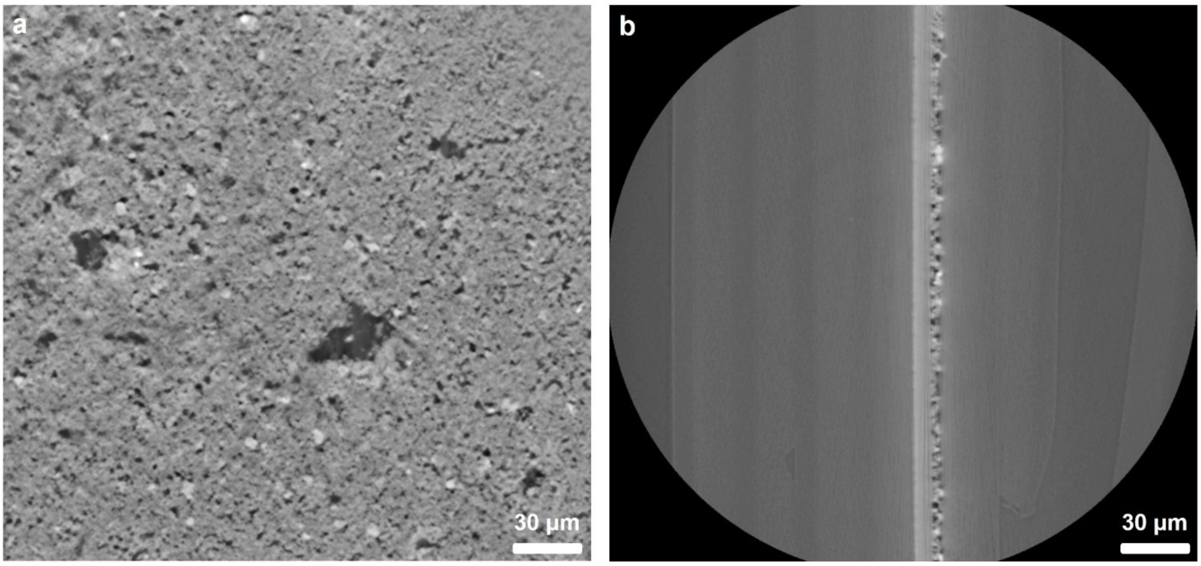

Fig. S11. XRM 2D images of the (a) *x-y* and (b) *y-z* planes of the pristine p-Ag-Ni layer.

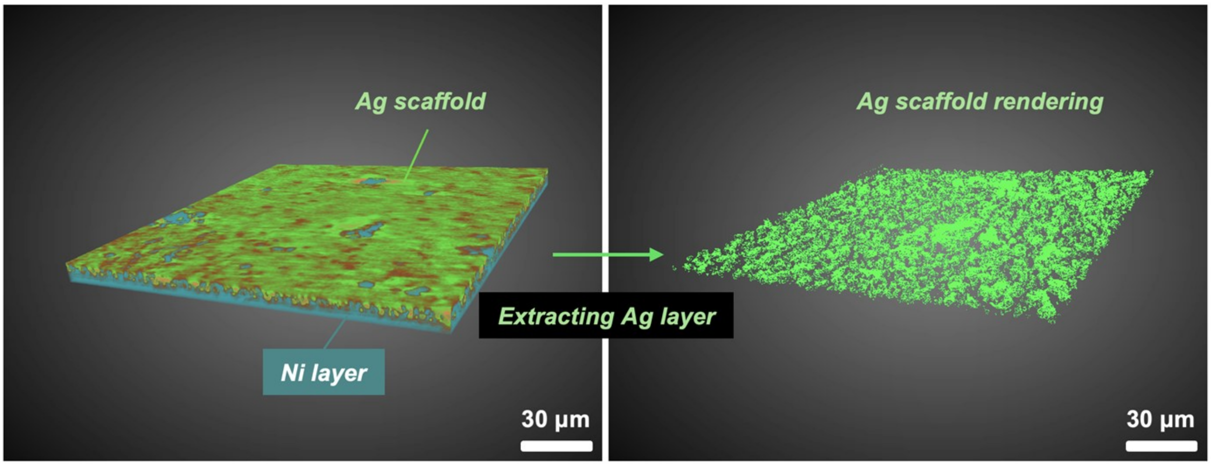

Fig. S12. XRM color mapping based on contrast variations in the pristine p-Ag-Ni layer.

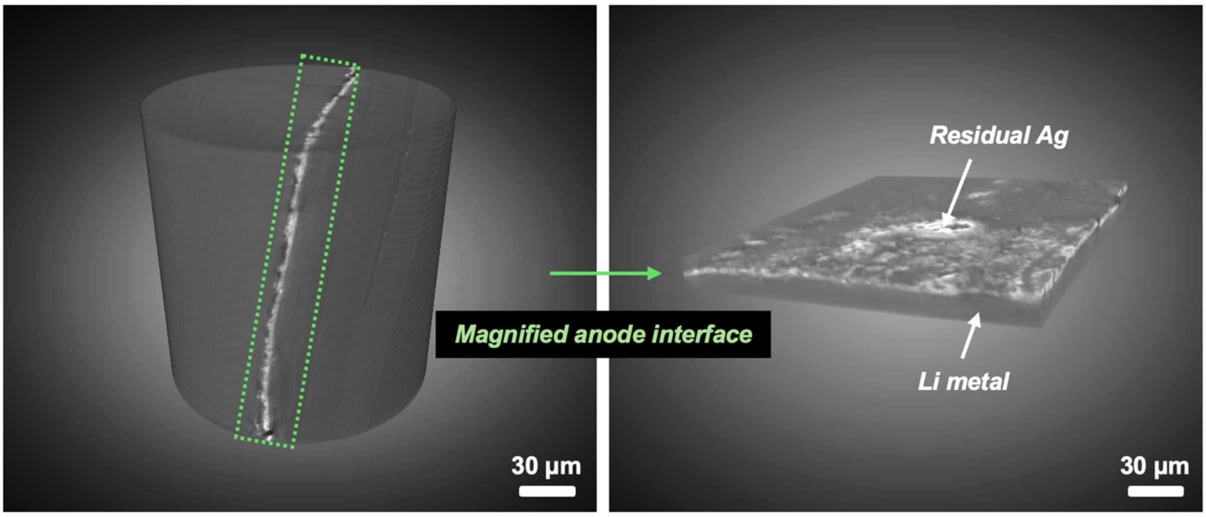

Fig. S13. XRM raw images of the p-Ag-Ni layer after Li plating of 3.5 mAh cm^{-2}.

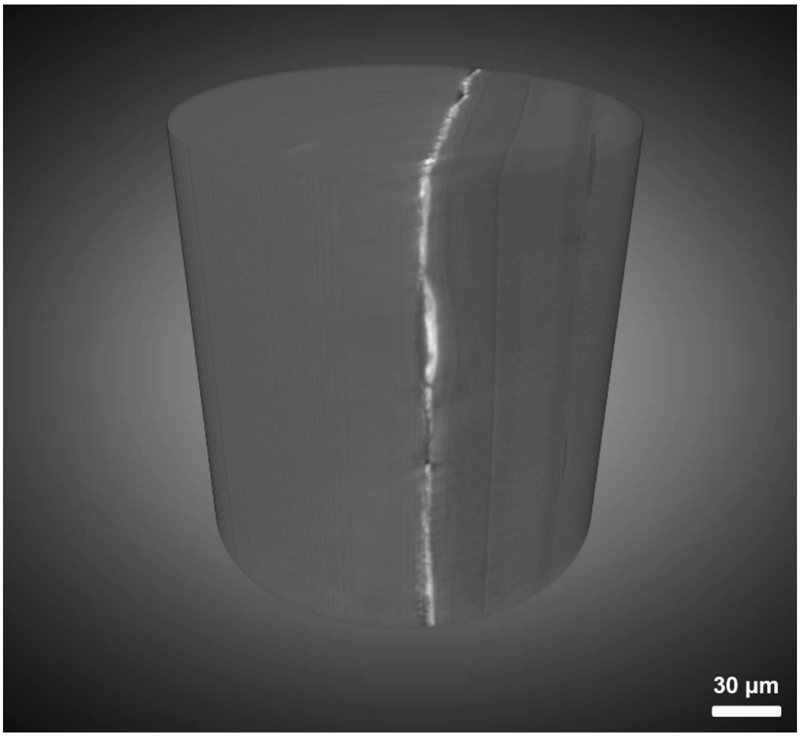

Fig. S14. XRM raw image of the p-Ag-Ni layer after 100 cycles of Li plating-stripping in the half-cell configuration.

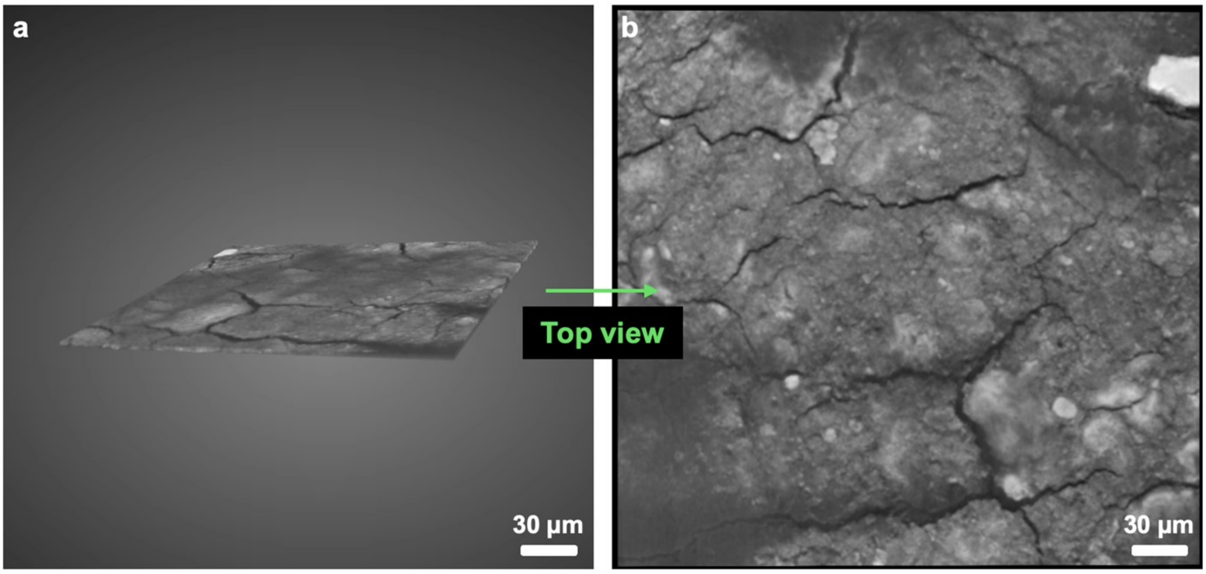

Fig. S15. XRM (a) 3D and (b) 2D magnified images of the p-Ag-Ni layer after 100 cycles of Li plating-stripping in the half-cell configuration.

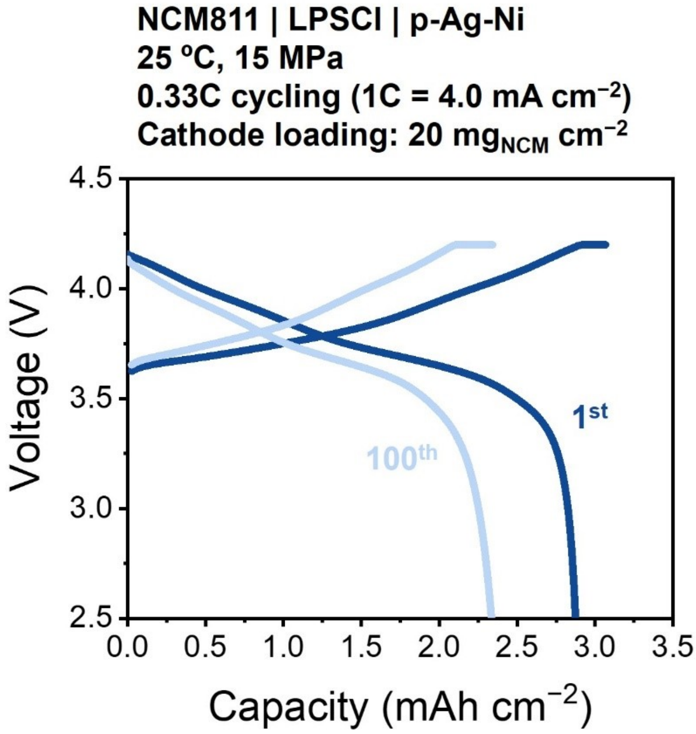

Fig. S16. Voltage profiles during full-cell evaluation with a high cathode loading of 20 mg cm^{-2}.

Table S1. Performance comparison of anode-less all-solid-state batteries employing sulfide-based electrolytes and an Ag-based interlayer.

	Solid electrolyte	**Capacity retention**	**Operating pressure**	**Operating temperature**	**Ref.**
p-Ag-Ni	Li_6PS_5Cl	84.0% @50 cyc	3 MPa	25 ºC	This work
Ag-Si	Li_6PS_5Cl	78.4% @200 cyc	30 MPa	50 ºC	1
Ag-C	Li_6PS_5Cl	~89% @1000 cyc	2 MPa	60 ºC	2
Ag-ZnO	Li_6PS_5Cl	80.8% @100 cyc	20 MPa	25 ºC	3
AgPEMA	Li_6PS_5Cl	80.6% @300 cyc	37 MPa	30 ºC	4
Ag-In	$Li_6PS_5Cl_{0.5}Br_{0.5}$	80.2% @250 cyc	30 MPa	25 ºC	5

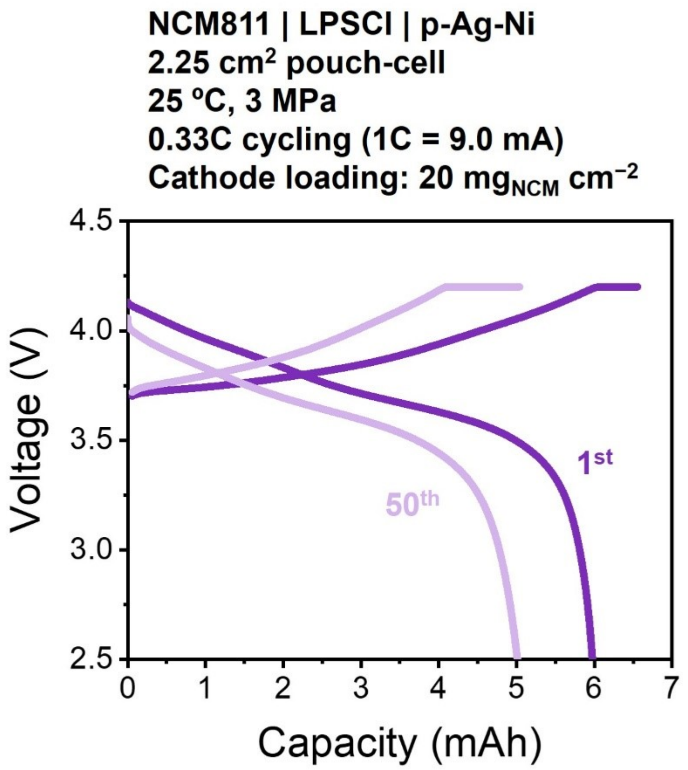

Fig. S17. Voltage profiles during pouch-cell evaluation with a high cathode loading of 20 mg cm^{-2}.

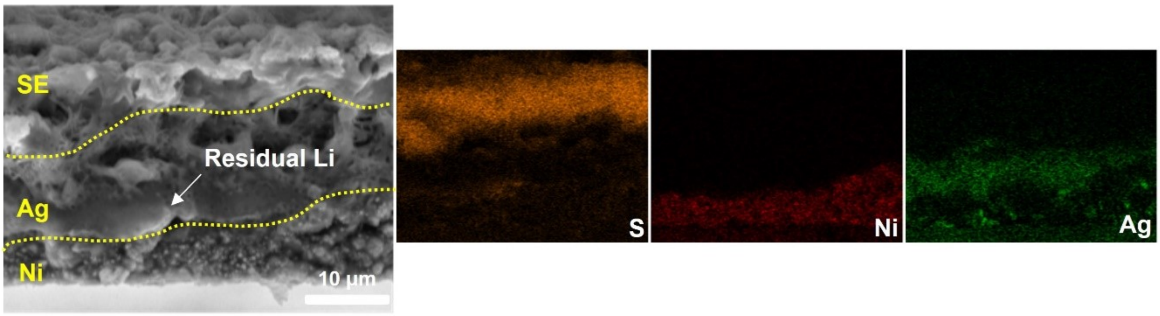

Fig. S18. Cross-sectional SEM-EDS images of the p-Ag-Ni anode interface after 30 cycles of pouch-cell operation under a low stack pressure of 3 MPa.

References (ESI†)

1. Y. Hwang, S.-Y. Kim, H. Yim, S.-H. Oh, J. H. Lee, Y. Kim, Y. Jeoun, S. H. Kim, J.-H. Lim, B. M. Weon, H. W. Jang, S.-H. Yu, Y.-E. Sung and J.-W. Choi, *ACS Energy Lett.*, 2026, **11**, 1769-1779.
2. Y.-G. Lee, S. Fujiki, C. Jung, N. Suzuki, N. Yashiro, R. Omoda, D.-S. Ko, T. Shiratsuchi, T. Sugimoto, S. Ryu, J. H. Ku, T. Watanabe, Y. Park, Y. Aihara, D. Im and I. T. Han, *Nat. Energy*, 2020, **5**, 299-308.
3. Y. Sohn, J. Oh, J. Lee, H. Kim, I. Hwang, G. Noh, T. Lee, J. Y. Kim, K. Y. Bae, T. Lee, N. Lee, W. J. Chung and J. W. Choi, *Adv. Mater.*, 2024, **36**, 2407443.
4. H.-T. Sim, M.-K. Oh, J.-B. Cho, C.-Y. Kim, S.-H. Kang, H.-G. Lee, Y.-S. Cho, S.-J. Park and D.-W. Kim, *Adv. Funct. Mater.*, 2025, e27688.
5. J. H. Lee, S.-H. Oh, H. Yim, H.-J. Lee, E. Kwon, S. Yu, J. S. Kim, J. Song, J. Koo, J. Cho, S. H. Kim, A. Ryu, S. H. Choi, Y. Kim, G. Im, J.-W. Choi and S.-H. Yu, *Energy Storage Mater.*, 2024, **69**, 103398.